
DreamCS: Geometry-Aware Text-to-3D Generation with Unpaired 3D Reward Supervision

Xiandong Zou¹, Ruihao Xia², Hongsong Wang³, Pan Zhou^{1*}

¹Singapore Management University ²East China University of Science and Technology

³Southeast University

Abstract

While text-to-3D generation has attracted growing interest, existing methods often struggle to produce 3D assets that align well with human preferences. Current preference alignment techniques for 3D content typically rely on hardly-collected preference-paired multi-view 2D images to train 2D reward models, when then guide 3D generation — leading to geometric artifacts due to their inherent 2D bias. To address these limitations, we construct 3D-MeshPref, the first large-scale unpaired 3D preference dataset, featuring diverse 3D meshes annotated by a large language model and refined by human evaluators. We then develop RewardCS, the first reward model trained directly on unpaired 3D-MeshPref data using a novel Cauchy-Schwarz divergence objective, enabling effective learning of human-aligned 3D geometric preferences without requiring paired comparisons. Building on this, we propose DreamCS, a unified framework that integrates RewardCS into text-to-3D pipelines — enhancing both implicit and explicit 3D generation with human preference feedback. Extensive experiments show DreamCS outperforms prior methods, producing 3D assets that are both geometrically faithful and human-preferred. Code and models will be released publicly.

1 Introduction

Text-to-3D generation has emerged as a key technique for automating 3D asset creation across domains such as digital comics, gaming, film, and virtual reality. Recent advancements include one-stage optimization-based 2D lifting strategies [1–10], two-stage 2D lifting methods that disentangle the modeling of geometry and appearance [3, 4], and inference-only 3D native methods [11, 12]. Despite these impressive advancements, generated 3D content often lacks alignment with human preference, underscoring the need for more robust and preference-aware generation frameworks.

To address this, reinforcement learning from human feedback (RLHF) [13–15] is introduced into the 3D generation pipeline [16–18], showing enhanced generative quality. However, these methods suffer from two core limitations that hinder their scalability and effectiveness. First, they rely on paired multi-view preference-labeled 2D: for each text prompt, multiple sets of preferred (winning) and dispreferred (losing) 2D renderings must be generated by rendering 3D assets from several camera positions and annotated by human experts. This process is computationally intensive, time-consuming and also expensive. More critically, given a text prompt, collecting its paired samples that contrast preferred and dispreferred views is inherently difficult and expensive, since only preferred and dispreferred pairs with sufficient preference gap are considered but are hardly generated in practice.

Second, these methods provide feedback only in 2D space, offering guidance based on image renderings rather than the 3D structure. This view-dependent supervision is inherently limited. As illustrated in Fig. 1a, a reward model trained on 2D multi-view data, such as ImageReward [19],

*Corresponding author.

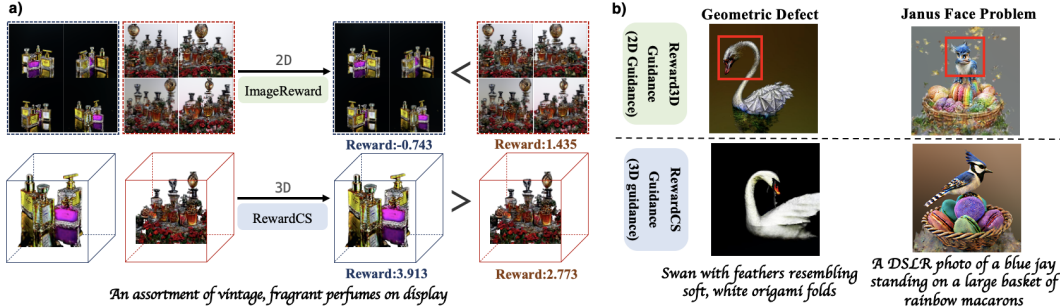


Figure 1: **Comparison between 2D- and 3D-based reward models.** a) 2D reward model ImageReward [19] assigns higher scores to 3D assets with geometric flaws, while our 3D reward model RewardCS accurately reflects human preference. b) Text-to-3D model DreamFusion [20] enhanced by 2D Reward3D [17] generates 3D assets with geometric defects and the Janus problem, while DreamFusion [20] with our RewardCS generates geometrically consistent 3D content.

may favor assets that appear plausible from certain angles while overlooking geometric flaws visible from others. During text-to-3D generation, as shown in Fig. 1b, 2D reward guidance, such as Reward3D [17], leads to geometric artifacts such as geometric defects and the Janus face problem, where a 3D object looks correct in one view but incorrect or distorted in another. The root cause of these issues is the lack of 3D-aware reward signals. Most current pipelines are built on diffusion-based 2D lifting techniques, which offer strong semantic guidance but lack supervision over global 3D geometry. Without an explicit understanding of the 3D structure, these models struggle to ensure consistency and plausibility across all viewpoints — ultimately limiting their real-world applicability.

Contributions. In this work, we take a step forward by proposing a novel 3D-reward guided framework for text-to-3D generation. To eliminate paired training data and provide geometry-level feedback during generation, we respectively resolve three associated key challenges by proposing the first large-scale preference-unpaired 3D dataset, the first 3D reward model trained on our dataset with theoretical guarantees, and the first 3D-reward guided text-to-3D generative framework.

Firstly, collecting paired preference-labeled 3D data is costly due to complex generation and annotation. To tackle this, we build **3D-MeshPref**, the first large-scale preference-unpaired 3D mesh dataset with 14,000+ samples, each sample containing a text prompt, 3D asset, and its preference reward score. We curate diverse and high-quality meshes from Cap3D [21], then use Llama-Mesh [22] to score geometric fidelity, semantic alignment, and structural plausibility, and finally refine these scores via human verification to ensure alignment with human judgments. Next, 3D assets with much higher rewards are selected as preferred, while those with lower rewards as dispreferred.

Secondly, a major constraint in training a 3D reward model on unpaired data is that prior preference alignment frameworks [13–15, 17, 18] typically rely on paired comparisons, and thus cannot operate effectively in unpaired settings. Accordingly, we propose **RewardCS**, the first 3D geometry-aware reward model trained on unpaired data. To enable learning from unpaired samples, we introduce a novel distribution-level training objective based on Cauchy-Schwarz (CS) divergence [23]. Rather than relying on direct pairwise comparisons, we treat embeddings of preferred and dispreferred assets as samples from two distributions and optimize the CS divergence between them. This encourages the model to assign higher rewards to geometrically and semantically superior 3D assets. Moreover, we prove that CS divergence on unpaired data is asymptotically equivalent to traditional paired preference supervision, offering theoretical justification for our unpaired reward learning paradigm.

Finally, existing text-to-3D frameworks lack native support for geometry-level feedback, posing significant integration challenges around mesh representation, differentiability, and reward model compatibility. Accordingly, we develop **DreamCS**, the first 3D-reward guided framework that integrates our RewardCS into existing text-to-3D pipelines. DreamCS works seamlessly with both implicit and explicit 3D representations through three key innovations: (1) differentiable meshization enabling end-to-end gradient flow from implicit fields; (2) adaptive mesh fusion that optimizes topology for RewardCS compatibility without sacrificing geometric detail; and (3) progressive reward guidance that automatically balances coarse structure refinement with fine-grained optimization.

Extensive experiments on the GPTEval3D benchmark [24] show that for both one-stage and two-stage text-to-3D generation pipelines like MVDream [1], Dreamfusion [20], and Magic3D [4], integrating

DreamCS into them achieves superior text-to-3D generation results in geometric alignment and mesh quality compared to previous multi-view guided methods. Moreover, our 3D reward guidance is complementary to existing 2D-based approaches, yielding further improvements when combined.

2 Related Work

Text-to-3D Generation. Recent advances in text-to-3D generation have largely been driven by the use of pretrained 2D diffusion models, given the scarcity and limited diversity of high-quality 3D datasets. A common strategy in works like DreamFusion [20] and SJC [5] involves using Score Distillation Sampling (SDS) to optimize 3D representations like NeRF [25]—by using gradients from a 2D diffusion model’s denoising process as supervision to refine the 3D scene. Unfortunately, SDS suffers from issues like view inconsistency, the Janus problem, and poor structural fidelity [2]. To mitigate these, new methods adopt either one-stage pipelines [1, 5, 9, 10] that jointly optimize geometry and appearance, or two-stage pipelines [2–4] that decouple them. However, most of them still struggle with alignment to human preferences, particularly in terms of global 3D geometry.

Learning from Human Feedback. Human feedback has become increasingly important in aligning generative models with user intent. In the language domain, RLHF [13, 14] and DPO [26] have successfully aligned LLM behavior to human values. These strategies have since been extended to multimodal domains, including image [19, 27] and video generation [28, 29]. In 3D generation, human feedback has only recently been incorporated. DreamReward [17] trains a multi-view image-based reward model using annotated 2D renderings for generation guidance. DreamDPO [18] applies DPO to refine 3D assets using human preferences collected from multi-view image comparisons. But these methods are inherently limited to 2D supervision, restricting alignment to view-specific appearance rather than global 3D structure and leading to inconsistent geometry. We address this gap by introducing RewardCS, a novel 3D reward model, for direct geometric supervision. We further design DreamCS framework to integrate geometry-aware human feedback from RewardCS into the optimization loop, ensuring better 3D consistency, plausibility, and human-aligned content.

3 Methodology

We first construct a large-scale preference-unpaired 3D mesh dataset, **3D-MeshPref**, in Section 3.1. Building on this, we develop the first 3D-geometry-aware reward model, **RewardCS**, trained on the 3D-MeshPref dataset, detailed in Section 3.2. To effectively integrate the 3D reward model, RewardCS, into text-to-3D generation pipelines, we propose **DreamCS** in Section 3.3 — a framework that aligns generated 3D content with human preferences through geometry-aware 3D supervision.

3.1 3D-MeshPref: Large-scale Preference-Unpaired 3D Mesh Dataset

A major challenge in 3D preference alignment is the lack of labeled datasets, as generating and annotating high-quality 3D assets is resource-intensive. Moreover, the complexity of explicit 3D representations hinders the construction of consistent paired preference data, limiting the development of effective 3D reward models. To overcome this, we propose **3D-MeshPref**, the first large-scale preference-unpaired 3D mesh dataset. It includes 14,000+ samples, each with a text prompt, 3D asset, and a preference reward score. Our pipeline combines automated LLM-based scoring with human refinement, enabling scalable annotation while preserving alignment with human judgment.

We build our dataset from annotated point clouds in Cap3D [21], sourced from 3D datasets like Objaverse [30] and ABO [31]. ABO contains high-resolution 3D household objects across 63 categories; Objaverse offers a large-scale and semantically rich 3D collection of over 21,000 categories. For diversity, we respectively collect 8,000 and 10,000 samples from ABO and Objaverse, which are then converted into high-quality mesh representations using MeshAnythingV2 [32]. To ensure mesh quality and compatibility with our 3D reward model, we apply QEM mesh simplification algorithm [33] to ensure the output with a maximum of 16,384 triangular faces. After filtering for mesh quality and completeness, we obtain 14,000+ 3D meshes.

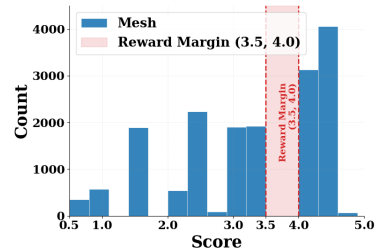


Figure 2: Annotated score distribution of meshes in **3D-MeshPref**.

We use Llama-Mesh [22], an LLM fine-tuned for 3D evaluation, to score each mesh on a 0-5 Likert scale [34] based on prompt alignment, structural realism, and visual fidelity. We observe that LLM-based ratings tend to overestimate quality relative to human perception. Accordingly, we

manually verify and correct them. See annotation guidelines in Appendix Sec. B. We then partition the dataset using a reward threshold (3.5-4.0): meshes scoring ≥ 4.0 show strong geometric integrity and semantic fidelity and are labeled as preferred (45% of all 3D asserts), while those ≤ 3.5 typically indicate structural defects or poor alignment with the prompt and are dispreferred (55%). This margin excludes ambiguous cases, ensuring reliable partitioning—a distribution visualized in Fig. 2.

3.2 RewardCS: 3D Geometry-aware Reward Model

Learning reward models for 3D assets is crucial for guiding high-quality text-to-3D generation [16, 17], but it is hindered by the scarcity of paired preference annotations, which are costly and hard to scale due to 3D complexity. Prior preference alignment methods — both general (e.g., DPO [26] and its variants [35, 36]) and 3D-specific [17, 18] — rely on paired data of the form $\{\mathbf{m}_i^+, \mathbf{m}_i^-, \mathbf{c}_i\}_{i=1}^m$, where each tuple includes a prompt \mathbf{c}_i drawn from prompt distribution p_C , and a pair of 3D meshes: a preferred one \mathbf{m}_i^+ and a dispreferred one \mathbf{m}_i^- . These samples are drawn from prompt-dependent distributions: $\mathbf{m}_i^+ \sim p^+(\cdot|\mathbf{c}_i)$ and $\mathbf{m}_i^- \sim p^-(\cdot|\mathbf{c}_i)$. The goal is to train reward models to assign higher rewards to preferred assets and thus guide text-to-3D generative models. However, this paradigm fails when such paired data are unavailable, which is common in real-world 3D settings.

3.2.1 RewardCS: A Novel Framework for Unpaired 3D Preference Learning

To overcome this limitation, we introduce **RewardCS**, the first geometry-aware 3D reward model that learns from unpaired preference data. Rather than relying on explicit preferred–dispreferred pairs, RewardCS leverages a distributional training objective based on Cauchy-Schwarz (CS) divergence [23], enabling effective preference modeling at scale. Our method is built upon the newly introduced 3D-MeshPref dataset, which contains only unpaired samples: high-quality (preferred) and low-quality (dispreferred) 3D meshes associated with diverse prompts.

Let $\{\mathbf{n}_i^+\}_{i=1}^m \sim p^+(\cdot|\mathbf{c}_i)$ and $\{\mathbf{n}_j^-\}_{j=1}^n \sim p^-(\cdot|\mathbf{c}_j)$ denote two sets of unpaired preferred and dispreferred 3D meshes, each conditioned on independently sampled prompts $\{\mathbf{c}_i\}_{i=1}^m$ and $\{\mathbf{c}_j\}_{j=1}^n$ from a distribution p_C . Standard preference alignment methods [13, 14, 17] are inapplicable in this unpaired setting because they require joint comparisons across samples from the same prompt. Instead, we formulate preference learning as a distribution matching problem.

We define a 3D reward model as a function $r_\theta : \mathcal{M} \times \mathcal{C} \rightarrow \mathbb{R}$, parameterized by θ , which maps a 3D mesh $\mathbf{m} \in \mathcal{M}$ and a text prompt embedding $\mathbf{c} \in \mathcal{C}$ to a scalar reward. Our reward model, RewardCS, consists of an encoder r_{θ_e} that transforms the input pair into a unified embedding $\mathbf{z} \in \mathcal{Z}$ and a projection head to generate a scalar reward. To train the 3D reward model, we encode unpaired preferred and dispreferred samples into latent embeddings via the text-to-3D model:

$$\{\mathbf{x}_i\}_{i=1}^m = r_{\theta_e}(\mathbf{n}_i^+, \mathbf{c}_i) \sim p(\mathbf{x}), \quad \{\mathbf{y}_j\}_{j=1}^n = r_{\theta_e}(\mathbf{n}_j^-, \mathbf{c}_j) \sim p(\mathbf{y}). \quad (1)$$

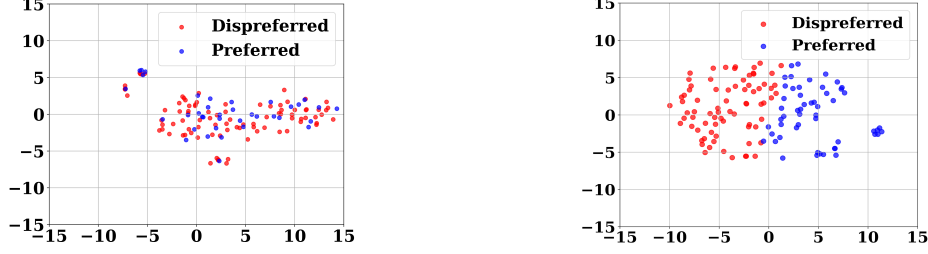
We treat these embeddings as samples from two distinct distributions $p(\mathbf{x})$ and $p(\mathbf{y})$, representing the overall structure of high- and low-quality 3D meshes in the latent space. Then rather than comparing individual mesh pairs, we aim to separate the distributions $p(\mathbf{x})$ and $p(\mathbf{y})$ in the embedding space. It allows the reward model to generalize over the global statistical properties of high- and low-quality 3D assets, enabling robust learning even when direct pairwise supervision is unavailable. To this end, we introduce a distribution-level loss based on CS divergence [37], which quantifies dissimilarity between two distributions in a symmetric and differentiable manner:

$$D_{CS}(p(\mathbf{x}) \| p(\mathbf{y})) = -\log \left(\left(\int p(\mathbf{x})p(\mathbf{y}) \, d\mathbf{x}d\mathbf{y} \right)^2 / \left(\int p(\mathbf{x})^2 \, d\mathbf{x} \int p(\mathbf{y})^2 \, d\mathbf{y} \right) \right). \quad (2)$$

Compared to the Kullback–Leibler divergence [38], the CS divergence offers a theoretically tighter CS divergence offers a tighter generalization bound [39] and is more robust than Jensen-Shannon divergence, which lacks a closed-form for Gaussians [40, 41]. This makes CS divergence well-suited for unpaired 3D reward learning, as maximizing it helps the model capture semantic and geometric cues that differentiate preferred from dispreferred assets without explicit supervision for each prompt.

Estimation of CS-Divergence. Since true data distribution densities $p(\mathbf{x})$ and $p(\mathbf{y})$ are unknown, we estimate them via kernel density estimation (KDE) [42]. Let $\{\mathbf{x}_i\}_{i=1}^m$ and $\{\mathbf{y}_j\}_{j=1}^n$ denote the embeddings of preferred and dispreferred samples, respectively. The empirical CS divergence is:

$$\hat{D}_{CS}(p(\mathbf{x}) \| p(\mathbf{y})) = \log \left(\frac{1}{m^2} \sum_{i,j=1}^m \kappa(\mathbf{x}_i, \mathbf{x}_j) \right) + \log \left(\frac{1}{m^2} \sum_{i,j=1}^n \kappa(\mathbf{y}_i, \mathbf{y}_j) \right) - 2 \log \left(\frac{1}{mn} \sum_{i=1}^m \sum_{j=1}^n \kappa(\mathbf{x}_i, \mathbf{y}_j) \right), \quad (3)$$



(a) RewardCS trained using Eq. (4) with $\lambda = 0$.

(b) RewardCS trained using Eq. (4) with $\lambda = 1$.

Figure 3: **t-SNE visualizations of class token embeddings based on different RewardCS in 3D-MeshPref data.** The addition of \mathcal{L}_{div} enables RewardCS to separate the underlying data distributions of preferred and dispreferred mesh samples ($p(\mathbf{x})$ and $p(\mathbf{y})$) in the learned embedding space.

where $\kappa(\cdot, \cdot)$ is a kernel function. This estimator possesses desirable properties: it is symmetric and differentiable. Importantly, it supports unequal numbers of preferred and dispreferred unpaired samples ($m \neq n$), enabling distributional alignment without requiring pairwise annotations.

Overall Training Objective of RewardCS. To train our RewardCS model r_θ , we combine a regression loss with the CS divergence loss. The final training objective is given by:

$$\mathcal{L}_{\text{RewardCS}}(\theta) = \mathcal{L}_{\text{MSE}}(\theta) + \lambda \mathcal{L}_{\text{div}}(\theta), \quad (4)$$

where \mathcal{L}_{MSE} is the mean squared error for reward prediction, $\mathcal{L}_{\text{div}} = -\hat{D}_{\text{CS}}(p(\mathbf{x}); p(\mathbf{y}))$ encourages separation between preferred and dispreferred mesh embedding distributions, and λ is a hyperparameter. Fig. 3 shows 2D t-SNE visualizations of mesh embeddings from RewardCS trained with $\lambda = 0$ and $\lambda = 1$. Adding \mathcal{L}_{div} helps the reward model distinguishing preferred and dispreferred meshes in the embedding space, and enables RewardCS to align with human preferences from unpaired data.

Theoretical Justification. We analyze CS divergence for training the 3D reward model on unpaired preference data by demonstrating its asymptotic equivalence to paired preference supervision. Optimizing the CS divergence is equivalent to optimizing a quantity in a kernel feature space [23, 37]:

$$\hat{D}_{\text{CS}}(p(\mathbf{x}) \| p(\mathbf{y})) = -2 \log \frac{\langle \boldsymbol{\mu}_x, \boldsymbol{\mu}_y \rangle_{\mathcal{H}}}{\|\boldsymbol{\mu}_x\|_{\mathcal{H}} \|\boldsymbol{\mu}_y\|_{\mathcal{H}}}, \quad \text{with} \quad \boldsymbol{\mu}_x = \frac{1}{m} \sum_{i=1}^m \varphi(\mathbf{x}_i), \quad \boldsymbol{\mu}_y = \frac{1}{n} \sum_{i=1}^n \varphi(\mathbf{y}_i), \quad (5)$$

where a characteristic kernel $\kappa(\mathbf{x}, \mathbf{y})$ is defined as $\kappa(\mathbf{x}, \mathbf{y}) = \langle \varphi(\mathbf{x}), \varphi(\mathbf{y}) \rangle_{\mathcal{H}}$, and φ maps samples to a Reproducing Kernel Hilbert Space (RKHS) \mathcal{H} [43]. In our case, we need to compute the means as

$$\begin{aligned} \boldsymbol{\mu}_x^{\text{paired}} &= \rho(\{(\mathbf{m}_i^+, \mathbf{c}_i)\}_{i=1}^m), & \boldsymbol{\mu}_y^{\text{paired}} &= \rho(\{(\mathbf{m}_i^-, \mathbf{c}_i)\}_{i=1}^m), \\ \boldsymbol{\mu}_x^{\text{unpaired}} &= \rho(\{(\mathbf{n}_i^+, \mathbf{c}_i)\}_{i=1}^m), & \boldsymbol{\mu}_y^{\text{unpaired}} &= \rho(\{(\mathbf{n}_j^-, \mathbf{c}_i)\}_{i=1}^n), \end{aligned} \quad (6)$$

where $\rho(\{(\mathbf{m}_i, \mathbf{c}_i)\}_{i=1}^k) = \frac{1}{k} \sum_{i=1}^k \varphi(r_{\theta_c}(\mathbf{m}_i, \mathbf{c}_i))$. Then we can define the CS divergence loss on unpaired data and paired data:

$$\hat{D}_{\text{CS}}^{\text{paired}} = -2 \log \frac{\langle \boldsymbol{\mu}_x^{\text{paired}}, \boldsymbol{\mu}_y^{\text{paired}} \rangle_{\mathcal{H}}}{\|\boldsymbol{\mu}_x^{\text{paired}}\|_{\mathcal{H}} \|\boldsymbol{\mu}_y^{\text{paired}}\|_{\mathcal{H}}}, \quad \hat{D}_{\text{CS}}^{\text{unpaired}} = -2 \log \frac{\langle \boldsymbol{\mu}_x^{\text{unpaired}}, \boldsymbol{\mu}_y^{\text{unpaired}} \rangle_{\mathcal{H}}}{\|\boldsymbol{\mu}_x^{\text{unpaired}}\|_{\mathcal{H}} \|\boldsymbol{\mu}_y^{\text{unpaired}}\|_{\mathcal{H}}}, \quad (7)$$

Then we pose necessary assumptions widely used in RLHF and divergence analysis [44–46].

Assumption 1. *a) The kernel $\kappa(\cdot, \cdot)$ is bounded, i.e. $\sup_{\mathbf{x}, \mathbf{y} \in \text{dom}(\kappa)} \kappa(\mathbf{x}, \mathbf{y}) \leq K$, and characteristic, meaning the kernel mean embedding is injective. b) The population mean embeddings of the preferred and dispreferred samples satisfy: $\|\boldsymbol{\mu}_x^{\text{paired}}\|_{\mathcal{H}}, \|\boldsymbol{\mu}_x^{\text{unpaired}}\|_{\mathcal{H}}, \|\boldsymbol{\mu}_y^{\text{paired}}\|_{\mathcal{H}}, \|\boldsymbol{\mu}_y^{\text{unpaired}}\|_{\mathcal{H}} > 0$.*

Assumption 1 (a) and (b) are standard assumptions in kernel methods [47–49], and hold in our case. We use the Gaussian kernel $\kappa_\sigma(\mathbf{x}, \mathbf{y}) = \exp(-\|\mathbf{x} - \mathbf{y}\|_2^2 / (2\sigma^2))$, which is bounded and characteristic, and our data distributions are well-separated, satisfying the non-zero mean embedding condition.

Theorem 1 (Asymptotic Equivalence). *Suppose Assumption 1 holds. With a constant $C > 0$, the empirical CS divergences $\hat{D}_{\text{CS}}^{\text{paired}}$ and $\hat{D}_{\text{CS}}^{\text{unpaired}}$ computed from paired and unpaired data satisfy:*

$$\left| \hat{D}_{\text{CS}}^{\text{paired}} - \hat{D}_{\text{CS}}^{\text{unpaired}} \right| \leq C \cdot \left(\frac{1}{\sqrt{m}} + \frac{1}{\sqrt{n}} \right) \xrightarrow{p} 0 \quad \text{as } m, n \rightarrow \infty, \quad (8)$$

See its proof in Appendix Sec. A. Thm.1 shows that the CS divergence computed from paired and unpaired preference data converges asymptotically at a convergence rate of $\mathcal{O}\left(\frac{1}{\sqrt{m}} + \frac{1}{\sqrt{n}}\right)$. Thus, our

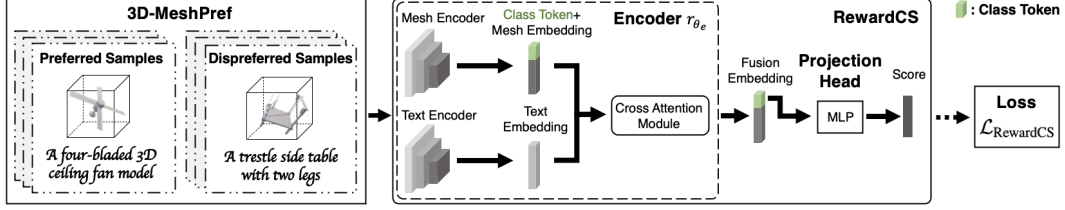


Figure 4: RewardCS is trained on 3D-MeshPref using Cauchy-Schwarz objective.

RewardCS can learn a latent embedding \mathbf{z} such that maximizing CS divergence between embeddings of preferred and dispreferred samples induces reward separation even without paired data.

3.2.2 Network Architecture of RewardCS

As shown in Fig. 4, RewardCS contains two key components: an encoder r_{θ_e} to produce a unified representations of 3D geometry and text, and a prediction head to generate a scalar reward score.

The encoder r_{θ_e} integrates three modules: a 3D mesh encoder for geometric feature extraction, a text encoder for prompt representation, and a cross-modal fusion module to integrate the two. 3D mesh encoder uses MeshMAE [50], a masked Vision Transformer (ViT) autoencoder for 3D meshes. Each input mesh is divided into 256 non-overlapping patches, with each patch consisting of 64 triangular faces. Each face is represented by a 10-dimensional feature vector capturing geometric attributes like area, angles, surface normals, and inner products between face and vertex normals. This strategy enables 3D mesh encoder to capture both localized surface details and global geometric context.

For text encoder, it adopts MeshCLIP [51] to map input text prompt into a sequence of semantic embeddings. To fuse mesh and text information, we apply a cross-attention mechanism: mesh tokens—including a learnable 128-dimensional class token prepended to the sequence—act as queries, while text tokens serve as keys and values. This design allows semantic guidance from the prompt to be injected into the geometric representation. The class token, which captures the global fused context, is then passed to an MLP-based projection head to produce the final reward score.

3.3 DreamCS: 3D Reward Guidance Framework

Integrating a 3D reward model into text-to-3D frameworks presents two key challenges. Firstly, existing reward methods are designed for 2D paired preferences and cannot directly handle preference-unpaired explicit 3D mesh representations, requiring a differentiable mechanism to convert implicit fields into mesh form. Secondly, meshes generated during training may not meet the reward model’s structural requirements due to face count constraints, necessitating adaptive topology alignment. To address these, we propose **DreamCS**, the first geometry-aware 3D reward guidance framework, integrating our RewardCS model into existing text-to-3D pipelines. As shown in Fig. 5, DreamCS enables end-to-end optimization via: (1) a differentiable meshization module for reward supervision, (2) an adaptive mesh fusion algorithm for topology alignment, and (3) a progressive reward guidance scheme balancing exploration and reward optimization.

Differentiable Meshization. Text-to-3D models often operate on implicit representations such as NeRF or SDFs, which must be converted into explicit mesh geometry to be compatible with our RewardCS model. Accordingly, we introduce a differentiable meshization module that enables smooth conversion from these fields to triangle meshes without breaking the optimization flow.

For pipelines based on SDS [20], we use DMTet [52] to extract high-quality isosurfaces in a differentiable way. This preserves the gradient flow from the reward signal back to the underlying implicit 3D parameters. Compared to Marching Cubes,

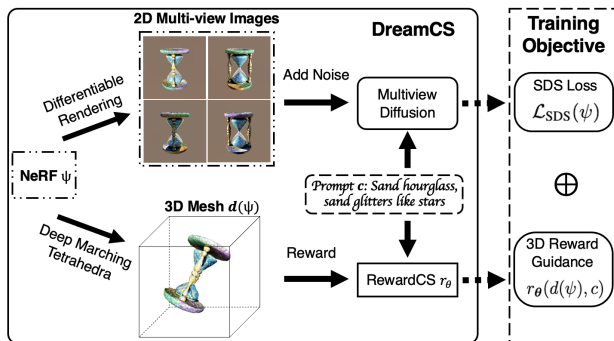


Figure 5: Overall framework of DreamCS: integrate RewardCS into the SDS framework for NeRF optimization.

DMTet enables high-fidelity geometry extraction. Regarding pipelines that natively optimize explicit meshes, this conversion step is bypassed, allowing for direct reward supervision.

Adaptive Mesh Fusion. Meshes produced above are often structurally incompatible with the input requirements of our reward model, RewardCS which expects meshes partitioned into 256 non-overlapping patches, each with 64 faces. To address this, we propose an adaptive mesh fusion algorithm that simplifies and reorganizes mesh topology while preserving geometric fidelity.

The algorithm iteratively merges adjacent faces using two criteria: (1) similarity in face normals and (2) topological adjacency (shared vertex). When two faces share a vertex and exhibit high normal similarity, we construct a new face using the shared vertex and one additional vertex from each original face. When two faces share an edge and have highly aligned normals, a new face is formed using the edge and a third vertex from either face. This fusion process reduces mesh complexity while maintaining fine structural details. Importantly, the entire fusion algorithm is differentiable and integrated into the training loop, maintaining gradient flow and supporting end-to-end learning.

Progressive Reward Guidance. To ensure faithful 3D generation, DreamCS integrates RewardCS through progressive guidance. At each optimization step, the current differentiable mesh — produced via our differentiable meshization module — is evaluated by the RewardCS model r_θ , which provides a gradient-based signal reflecting its geometric plausibility and alignment with the input prompt.

Let the 3D generation be parameterized by an implicit representation ψ . At each optimization step, the mesh $d(\psi)$ derived from ψ via DMTet is evaluated by the reward model r_θ to assign a scalar score that reflects mesh’s quality w.r.t. the input prompt c . The optimization objective is defined as:

$$\mathcal{L}(\psi) = \mathcal{L}_{\text{SDS}}(\psi) - \alpha \cdot r_\theta(d(\psi), c), \quad (9)$$

where \mathcal{L}_{SDS} is vanilla score distillation loss [20], and α gradually increases to strength the reward signal. Rather than applying a fixed reward weight throughout training, we use a coarse-to-fine scheduling strategy: early in training, α is kept low to allow broad exploration of shape space; later, it increases to enforce stricter alignment with the preferences encoded in RewardCS. This dynamic schedule encourages diversity in the early stages and precise refinement in the later stages.

4 Experiment

Setup. We test our DreamCS by integrating our reward model RewardCS into one-stage SDS-based text-to-3D generative models like MVDream [1] and DreamFusion [20], and two-stage models like Magic3D [4] and Fantasia3D [3]. Moreover, we compare with other 3D preference alignment approaches, DreamReward [17], and DreamDPO [18]. All baselines use their official implementations where available, otherwise Threestudio’s implementation [53]. Our DreamCS is initialized by pretrained ShapeNet [54] and fine-tuned on 3D-MeshPref by minimizing loss (4). All methods run for 20,000 steps, with an additional 10,000 steps for refinement in texture/geometry-aware baselines. Rendering resolution follows a coarse-to-fine schedule (64×64 for the first 5,000 steps, then 256×256), and DreamCS’s α linearly increases from 10 to 20 during generation.

We use all 110 prompts in GPTEval3D [24] for evaluation. We assess texture and geometry quality using ImageReward (IR) [19] and VisionReward (VR) [55] on rendered 2D images. We proposed a 3D Geometry-Asset Alignment Reward (GA) metric based on RewardCS trained with a different training configuration. It serves as an independent evaluator for 3D geometry-text alignment. MiniCPM-o [10], a multimodal vision-language model, rates text-asset alignment, 3D plausibility, and geometry-texture consistency on a 0–5 Likert scale. Finally, a user study with 30 participants on 30 prompts assesses these criteria. See more details in Appendix B.

Quantitative Comparison. Tables 1 and 2 present a comparative analysis of one-stage (DreamFusion, MVDream) and two-stage (Magic3D, Fantasia3D) pipelines, along with their respective 2D-guided (Reward3D, DreamDPO) and our proposed 3D-guided (RewardCS) variants. Notably, Table 2 specifically compares with DreamDPO, as it only reported results on MVDream and did not release code and model, and we follow its setting to test ours for comparison. As Reward3D [17] is finetuned to optimize ImageReward score. So methods with Reward3D guidance often overfit the ImageReward (IR) metric, but do not generate high-quality 3D assets as shown in Fig. 6 (see discussion below).

Three key findings emerge from these results. **1)** RewardCS consistently improves upon all vanilla baselines and outperforms 2D-guided variants in both GA and VR scores. In Magic3D, RewardCS achieves the highest GA (3.21), significantly outperforming the baseline (2.66) and the variant with 2D guidance (2.54), while achieving the highest VR score (-1.57). Similarly, in DreamFusion,

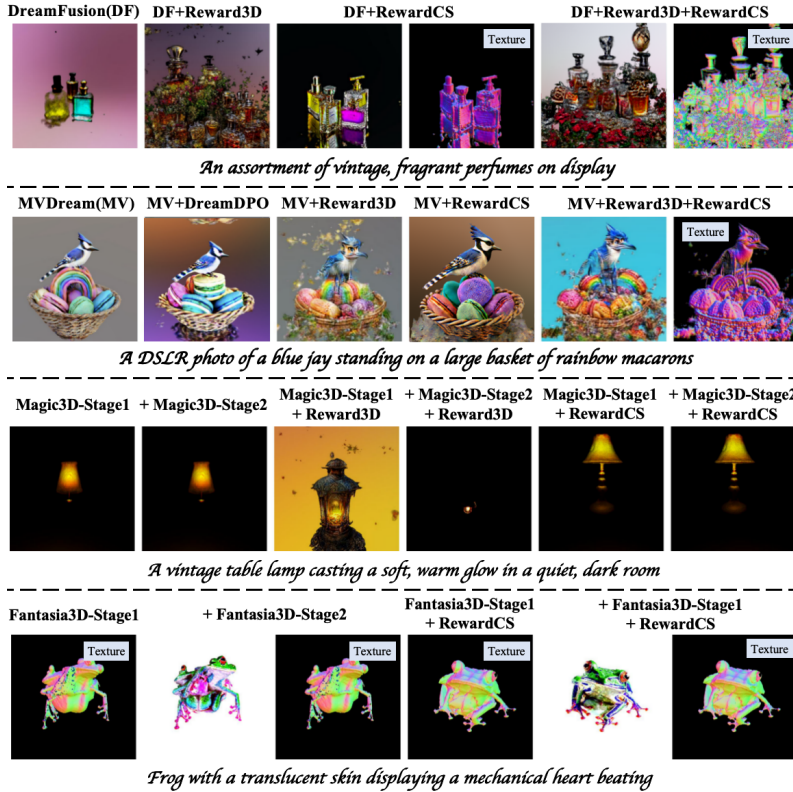


Figure 6: Qualitative comparisons with 1-stage generation pipelines (DreamFusion and MVDream) and 2-stage generation pipelines (Magic3D and Fantasia3D). More visualizations are in Appendix C

Table 1: Comparison of baselines using 110 GPTEval 3D prompts under **12 multi-view** images. Metrics: IR = ImageReward, VR = VisionReward, GA = 3D Geometry-Asset Alignment Reward.

| Method | IR \uparrow | VR \uparrow | GA \uparrow | Method | IR \uparrow | VR \uparrow | GA \uparrow |
|--------------------|---------------|---------------|---------------|--------------------------|---------------|---------------|---------------|
| DreamFusion | -0.86 | -3.22 | 2.52 | Magic3D Stage1 | -1.21 | -3.25 | 2.47 |
| +Reward3D | 1.72 | -3.12 | 2.76 | +Magic3D Stage2 | -0.96 | -3.02 | 2.66 |
| +RewardCS | -0.22 | -2.10 | 2.97 | Magic3D Stage1+Reward3D | 1.04 | -3.10 | 2.86 |
| +Reward3D+RewardCS | 1.88 | -2.78 | 3.21 | +Magic3D Stage2+Reward3D | -0.62 | -3.31 | 2.54 |
| MVDream | -0.52 | -3.30 | 2.78 | Magic3D Stage1+RewardCS | -0.72 | -1.89 | 3.01 |
| +Reward3D | 1.95 | -3.13 | 2.88 | +Magic3D Stage2+RewardCS | -0.52 | -1.57 | 3.21 |
| +RewardCS | -0.43 | -2.10 | 2.95 | Fantasia3D | -1.10 | -3.04 | 2.94 |
| +Reward3D+RewardCS | 1.98 | -1.91 | 3.09 | +RewardCS | -0.74 | -1.02 | 3.34 |

RewardCS leads with a GA score of 2.97, surpassing both baseline (2.52) and the variant with 2D guidance (2.76), and the best VR score (-2.10). **2)** RewardCS exhibits strong compatibility with diverse text-to-3D backbones, including both implicit 3D representation optimization and explicit mesh-based rendering pipelines. In MVDream, it improves the vanilla baseline from -3.30 to -2.10 in VR score and from 2.78 to 2.95 in GA score, outperforming the Reward3D variant (-3.13 VR, 2.88 GA). Furthermore, in Fantasia3D’s mesh-rendering-based pipeline, RewardCS achieves the highest GA score and significantly improves the VR from -3.04 to -1.02. **3)** 3D and 2D guidance prove complementary: integrated guidance in DreamFusion achieves peak IR (1.88) and GA (3.21) scores while improving VR to -2.78, demonstrating that Reward3D enhances multi-view consistency while RewardCS optimizes geometric alignment.

Visualization Comparison. Fig. 6 compares visual generation results. Vanilla baselines like DreamFusion frequently exhibit textural misalignment and the Janus face problem. While baselines with 2D guidance via Reward3D or DreamDPO show improved aesthetics, they still produce noticeable geometric artifacts. In contrast, our DreamCS framework (baseline + our RewardCS) demonstrates robust compatibility with both implicit and explicit generation paradigms, consistently delivering 3D assets with superior text alignment, geometric consistency, and texture fidelity. Moreover, our RewardCS is also orthogonal to 2D guidance like Reward3D to further enhance text-to-3D generation.

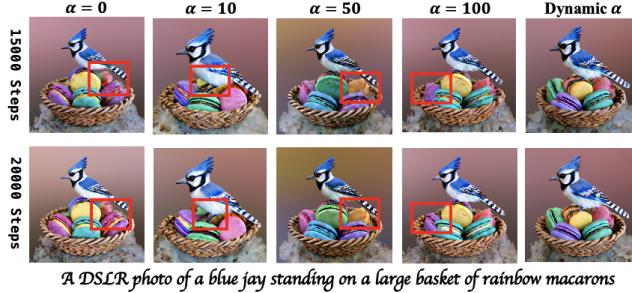


Figure 7: Ablation study on the weight of 3D guidance α in MVDream at 15000 and 20000 steps.

Table 2: Comparison of baselines using 110 GPTEval 3D prompts under **4 multi-view** images.

| Method | ImageReward \uparrow | Vision Reward \uparrow |
|--------------------|------------------------|--------------------------|
| MVdream | -0.51 | -3.18 |
| +Reward3D | 1.96 | -3.13 |
| +DreamDPO | -0.35 | N.A. |
| +RewardCS | -0.42 | -1.99 |
| +Reward3D+RewardCS | 2.02 | -1.53 |

Evaluation via MiniCPM-o and Human. Tab. 3 (a) reports evaluation results using MiniCPM-o, and Tab. 3 (b) reports findings from a user study. One can observe that RewardCS guidance outperforms 2D preference-based methods on geometry-related criteria while maintaining competitive performance in text-asset alignment. In MiniCPM-o evaluations, MVDream with RewardCS achieves the highest scores in 3D Plausibility (4.09) and G-T Alignment (4.02), significantly exceeding both MVDream and MVDream with Reward3D. User studies confirm this trend, with RewardCS again leading in 3D Plausibility (3.69) and G-T Alignment (3.65).

Table 3: Comparison of methods on MiniCPM-o evaluation (left) and user study (right) using (a) 110 and (b) 30 representative GPTEval3D prompts, respectively. Metrics: T-A = Text-Asset Alignment, 3DP = 3D Plausibility, G-T = Geometry-Texture Alignment.

| (a) MiniCPM-o evaluation on 110 prompts | | | | (b) User study on 30 prompts | | | |
|---|----------------|----------------|----------------|------------------------------|----------------|----------------|----------------|
| Method | T-A \uparrow | 3DP \uparrow | G-T \uparrow | Method | T-A \uparrow | 3DP \uparrow | G-T \uparrow |
| MVdream | 3.01 | 3.08 | 3.05 | MVdream | 2.84 | 2.93 | 2.89 |
| +Reward3D | 3.54 | 3.39 | 3.16 | +Reward3D | 3.08 | 3.19 | 3.02 |
| +RewardCS | 3.21 | 4.09 | 4.02 | +RewardCS | 3.27 | 3.69 | 3.65 |
| +Reward3D+RewardCS | 3.67 | 3.93 | 3.85 | +Reward3D+RewardCS | 3.34 | 3.54 | 3.48 |

Ablation Study. Fig. 7 shows the effect of varying guidance weight α in Eq. (9), balancing the 2D diffusion distillation score and DreamCS 3D guidance, on the quality of generated 3D assets using the MVDream backbone. Low values of α (0, 10) cause geometric ambiguity, while high α (50, 100) results in structural distortions. Our progressive strategy achieves a better balance between semantic accuracy and structural coherence, yielding improved results.

5 Conclusion

In this paper, we present DreamCS, the first 3D-guided text-to-3D generation framework explicitly designed for human preference alignment. Specifically, we construct a preference dataset on mesh data, 3D-MeshPref. Then we train a 3D reward model, RewardCS, on this dataset to encode human-aligned geometric priors. By incorporating RewardCS into the 3D generation pipeline, DreamCS produces geometrically plausible and texture-consistent 3D assets that are faithfully aligned with human preferences. Extensive experiments demonstrate that DreamCS consistently outperforms both vanilla and 2D-guided baselines across 3D geometry-oriented metrics and human evaluations.

Limitations. Due to limited budget, our evaluation of 3D generation relies on open-source LLMs like MiniCPM-o. Incorporating stronger models like GPT-4 [24] may yield more reliable and fine-grained feedback, and will be considered when budget becomes available. In addition, while DreamCS shows promising results, its performance is limited by base text-to-3D pipelines like DreamFusion. In future work, we plan to explore advanced text-to-3D backbones. See Broader Impact in Appendix.

References

- [1] Yichun Shi, Peng Wang, Jianglong Ye, Mai Long, Kejie Li, and Xiao Yang. Mvdream: Multi-view diffusion for 3d generation. *arXiv preprint arXiv:2308.16512*, 2023. 1, 2, 3, 7
- [2] Zhengyi Wang, Cheng Lu, Yikai Wang, Fan Bao, Chongxuan Li, Hang Su, and Jun Zhu. Pro-lificdreamer: High-fidelity and diverse text-to-3d generation with variational score distillation. *Advances in Neural Information Processing Systems*, 36:8406–8441, 2023. 3
- [3] Rui Chen, Yongwei Chen, Ningxin Jiao, and Kui Jia. Fantasia3d: Disentangling geometry and appearance for high-quality text-to-3d content creation. In *Proceedings of the IEEE/CVF international conference on computer vision*, pages 22246–22256, 2023. 1, 7
- [4] Chen-Hsuan Lin, Jun Gao, Luming Tang, Towaki Takikawa, Xiaohui Zeng, Xun Huang, Karsten Kreis, Sanja Fidler, Ming-Yu Liu, and Tsung-Yi Lin. Magic3d: High-resolution text-to-3d content creation. In *Proceedings of the IEEE/CVF conference on computer vision and pattern recognition*, pages 300–309, 2023. 1, 2, 3, 7
- [5] Haochen Wang, Xiaodan Du, Jiahao Li, Raymond A Yeh, and Greg Shakhnarovich. Score jacobian chaining: Lifting pretrained 2d diffusion models for 3d generation. In *Proceedings of the IEEE/CVF conference on computer vision and pattern recognition*, pages 12619–12629, 2023. 3
- [6] Ruoshi Liu, Rundi Wu, Basile Van Hoorick, Pavel Tokmakov, Sergey Zakharov, and Carl Vondrick. Zero-1-to-3: Zero-shot one image to 3d object. In *Proceedings of the IEEE/CVF international conference on computer vision*, pages 9298–9309, 2023.
- [7] Ruoxi Shi, Hansheng Chen, Zhuoyang Zhang, Minghua Liu, Chao Xu, Xinyue Wei, Linghao Chen, Chong Zeng, and Hao Su. Zero123++: a single image to consistent multi-view diffusion base model. *arXiv preprint arXiv:2310.15110*, 2023.
- [8] Guocheng Qian, Jinjie Mai, Abdullah Hamdi, Jian Ren, Aliaksandr Siarohin, Bing Li, Hsin-Ying Lee, Ivan Skorokhodov, Peter Wonka, Sergey Tulyakov, et al. Magic123: One image to high-quality 3d object generation using both 2d and 3d diffusion priors. *arXiv preprint arXiv:2306.17843*, 2023.
- [9] Zike Wu, Pan Zhou, Xuanyu Yi, Xiaoding Yuan, and Hanwang Zhang. Consistent3d: Towards consistent high-fidelity text-to-3d generation with deterministic sampling prior. In *Proceedings of the IEEE/CVF Conference on Computer Vision and Pattern Recognition*, pages 9892–9902, 2024. 3
- [10] Junzhe Zhu, Peiye Zhuang, and Sanmi Koyejo. Hifa: High-fidelity text-to-3d generation with advanced diffusion guidance. *arXiv preprint arXiv:2305.18766*, 2023. 1, 3
- [11] Christina Tsalicoglou, Fabian Manhardt, Alessio Tonioni, Michael Niemeyer, and Federico Tombari. Textmesh: Generation of realistic 3d meshes from text prompts. In *2024 International Conference on 3D Vision (3DV)*, pages 1554–1563. IEEE, 2024. 1
- [12] Heewoo Jun and Alex Nichol. Shap-e: Generating conditional 3d implicit functions. *arXiv preprint arXiv:2305.02463*, 2023. 1
- [13] Long Ouyang, Jeffrey Wu, Xu Jiang, Diogo Almeida, Carroll Wainwright, Pamela Mishkin, Chong Zhang, Sandhini Agarwal, Katarina Slama, Alex Ray, et al. Training language models to follow instructions with human feedback. *Advances in neural information processing systems*, 35:27730–27744, 2022. 1, 2, 3, 4
- [14] Paul F Christiano, Jan Leike, Tom Brown, Miljan Martic, Shane Legg, and Dario Amodei. Deep reinforcement learning from human preferences. *Advances in neural information processing systems*, 30, 2017. 3, 4
- [15] Kai Yang, Jian Tao, Jiafei Lyu, Chunjiang Ge, Jiabin Chen, Weihang Shen, Xiaolong Zhu, and Xiu Li. Using human feedback to fine-tune diffusion models without any reward model. In *Proceedings of the IEEE/CVF Conference on Computer Vision and Pattern Recognition*, pages 8941–8951, 2024. 1, 2

- [16] Desai Xie, Jiahao Li, Hao Tan, Xin Sun, Zhixin Shu, Yi Zhou, Sai Bi, Sören Pirk, and Arie E Kaufman. Carve3d: Improving multi-view reconstruction consistency for diffusion models with rl finetuning. In *Proceedings of the IEEE/CVF Conference on Computer Vision and Pattern Recognition*, pages 6369–6379, 2024. 1, 4
- [17] Junliang Ye, Fangfu Liu, Qixiu Li, Zhengyi Wang, Yikai Wang, Xinzhou Wang, Yueqi Duan, and Jun Zhu. Dreamreward: Text-to-3d generation with human preference. In *European Conference on Computer Vision*, pages 259–276. Springer, 2024. 2, 3, 4, 7
- [18] Zhenglin Zhou, Xiaobo Xia, Fan Ma, Hehe Fan, Yi Yang, and Tat-Seng Chua. Dreamdpo: Aligning text-to-3d generation with human preferences via direct preference optimization. *arXiv preprint arXiv:2502.04370*, 2025. 1, 2, 3, 4, 7
- [19] Jiazheng Xu, Xiao Liu, Yuchen Wu, Yuxuan Tong, Qinkai Li, Ming Ding, Jie Tang, and Yuxiao Dong. Imagereward: Learning and evaluating human preferences for text-to-image generation. *Advances in Neural Information Processing Systems*, 36:15903–15935, 2023. 1, 2, 3, 7
- [20] Ben Poole, Ajay Jain, Jonathan T Barron, and Ben Mildenhall. Dreamfusion: Text-to-3d using 2d diffusion. *arXiv preprint arXiv:2209.14988*, 2022. 2, 3, 6, 7
- [21] Tiange Luo, Chris Rockwell, Honglak Lee, and Justin Johnson. Scalable 3d captioning with pretrained models. *Advances in Neural Information Processing Systems*, 36:75307–75337, 2023. 2, 3, 19
- [22] Zhengyi Wang, Jonathan Lorraine, Yikai Wang, Hang Su, Jun Zhu, Sanja Fidler, and Xiaohui Zeng. Llama-mesh: Unifying 3d mesh generation with language models. *arXiv preprint arXiv:2411.09595*, 2024. 2, 3
- [23] Robert Jenssen, Jose C Principe, Deniz Erdogmus, and Torbjørn Eltoft. The cauchy–schwarz divergence and parzen windowing: Connections to graph theory and mercer kernels. *Journal of the Franklin Institute*, 343(6):614–629, 2006. 2, 4, 5
- [24] Tong Wu, Guandao Yang, Zhibing Li, Kai Zhang, Ziwei Liu, Leonidas Guibas, Dahua Lin, and Gordon Wetzstein. Gpt-4v (ision) is a human-aligned evaluator for text-to-3d generation. In *Proceedings of the IEEE/CVF conference on computer vision and pattern recognition*, pages 22227–22238, 2024. 2, 7, 9
- [25] Ben Mildenhall, Pratul P Srinivasan, Matthew Tancik, Jonathan T Barron, Ravi Ramamoorthi, and Ren Ng. Nerf: Representing scenes as neural radiance fields for view synthesis. *Communications of the ACM*, 65(1):99–106, 2021. 3
- [26] Rafael Rafailov, Archit Sharma, Eric Mitchell, Christopher D Manning, Stefano Ermon, and Chelsea Finn. Direct preference optimization: Your language model is secretly a reward model. *Advances in Neural Information Processing Systems*, 36:53728–53741, 2023. 3, 4
- [27] Youwei Liang, Junfeng He, Gang Li, Peizhao Li, Arseniy Klimovskiy, Nicholas Carolan, Jiao Sun, Jordi Pont-Tuset, Sarah Young, Feng Yang, et al. Rich human feedback for text-to-image generation. In *Proceedings of the IEEE/CVF Conference on Computer Vision and Pattern Recognition*, pages 19401–19411, 2024. 3
- [28] Xun Wu, Shaohan Huang, Guolong Wang, Jing Xiong, and Furu Wei. Boosting text-to-video generative model with mllms feedback. In *The Thirty-eighth Annual Conference on Neural Information Processing Systems*, 2024. 3
- [29] Jie Liu, Gongye Liu, Jiajun Liang, Ziyang Yuan, Xiaokun Liu, Mingwu Zheng, Xiele Wu, Qiulin Wang, Wenyu Qin, Menghan Xia, et al. Improving video generation with human feedback. *arXiv preprint arXiv:2501.13918*, 2025. 3
- [30] Matt Deitke, Dustin Schwenk, Jordi Salvador, Luca Weihs, Oscar Michel, Eli VanderBilt, Ludwig Schmidt, Kiana Ehsani, Aniruddha Kembhavi, and Ali Farhadi. Objaverse: A universe of annotated 3d objects. In *Proceedings of the IEEE/CVF conference on computer vision and pattern recognition*, pages 13142–13153, 2023. 3

- [31] Jasmine Collins, Shubham Goel, Kenan Deng, Achleshwar Luthra, Leon Xu, Erhan Gundogdu, Xi Zhang, Tomas F Yago Vicente, Thomas Dideriksen, Himanshu Arora, et al. Abo: Dataset and benchmarks for real-world 3d object understanding. In *Proceedings of the IEEE/CVF conference on computer vision and pattern recognition*, pages 21126–21136, 2022. 3
- [32] Yiwen Chen, Yikai Wang, Yihao Luo, Zhengyi Wang, Zilong Chen, Jun Zhu, Chi Zhang, and Guosheng Lin. Meshanything v2: Artist-created mesh generation with adjacent mesh tokenization. *arXiv preprint arXiv:2408.02555*, 2024. 3, 16
- [33] Yong Wu, Yuanjun He, and Hongming Cai. Qem-based mesh simplification with global geometry features preserved. In *Proceedings of the 2nd international conference on Computer graphics and interactive techniques in Australasia and South East Asia*, pages 50–57, 2004. 3
- [34] Ankur Joshi, Saket Kale, Satish Chandel, and D Kumar Pal. Likert scale: Explored and explained. *British journal of applied science & technology*, 7(4):396, 2015. 3
- [35] Yu Meng, Mengzhou Xia, and Danqi Chen. Simpo: Simple preference optimization with a reference-free reward. *Advances in Neural Information Processing Systems*, 37:124198–124235, 2024. 4
- [36] Xin Lai, Zhuotao Tian, Yukang Chen, Senqiao Yang, Xiangru Peng, and Jiaya Jia. Step-dpo: Step-wise preference optimization for long-chain reasoning of llms. *arXiv preprint arXiv:2406.18629*, 2024. 4
- [37] Wenzhe Yin, Zehao Xiao, Pan Zhou, Shujian Yu, Jiayi Shen, Jan-Jakob Sonke, and Efstratios Gavves. Distributional vision-language alignment by cauchy-schwarz divergence. *arXiv preprint arXiv:2502.17028*, 2025. 4, 5
- [38] Tim Van Erven and Peter Harremoës. Rényi divergence and kullback-leibler divergence. *IEEE Transactions on Information Theory*, 60(7):3797–3820, 2014. 4
- [39] Wenzhe Yin, Shujian Yu, Yicong Lin, Jie Liu, Jan-Jakob Sonke, and Efstratios Gavves. Domain adaptation with cauchy-schwarz divergence. *arXiv preprint arXiv:2405.19978*, 2024. 4
- [40] Bent Fuglede and Flemming Topsøe. Jensen-shannon divergence and hilbert space embedding. In *International symposium on information theory, 2004. ISIT 2004. Proceedings.*, page 31. IEEE, 2004. 4
- [41] Frank Nielsen. On the jensen–shannon symmetrization of distances relying on abstract means. *Entropy*, 21(5):485, 2019. 4
- [42] Stanisław Węglarczyk. Kernel density estimation and its application. In *ITM web of conferences*, volume 23, page 00037. EDP Sciences, 2018. 4
- [43] Alex Smola, Arthur Gretton, Le Song, and Bernhard Schölkopf. A hilbert space embedding for distributions. In *International conference on algorithmic learning theory*, pages 13–31. Springer, 2007. 5, 14
- [44] Banghua Zhu, Michael Jordan, and Jiantao Jiao. Principled reinforcement learning with human feedback from pairwise or k-wise comparisons. In *International Conference on Machine Learning*, pages 43037–43067. PMLR, 2023. 5
- [45] Xiandong Zou, Wanyu Lin, Yuchen Li, and Pan Zhou. Hps: Hard preference sampling for human preference alignment. *arXiv preprint arXiv:2502.14400*, 2025.
- [46] Taehyeon Kim, Jaehoon Oh, NakYil Kim, Sangwook Cho, and Se-Young Yun. Comparing kullback-leibler divergence and mean squared error loss in knowledge distillation. *arXiv preprint arXiv:2105.08919*, 2021. 5
- [47] Thomas Hofmann, Bernhard Schölkopf, and Alexander J Smola. Kernel methods in machine learning. 2008. 5
- [48] Arthur Gretton, Karsten Borgwardt, Malte Rasch, Bernhard Schölkopf, and Alex Smola. A kernel method for the two-sample-problem. *Advances in neural information processing systems*, 19, 2006.

- [49] Krikamol Muandet, Kenji Fukumizu, Bharath Sriperumbudur, Bernhard Schölkopf, et al. Kernel mean embedding of distributions: A review and beyond. *Foundations and Trends® in Machine Learning*, 10(1-2):1–141, 2017. 5
- [50] Yaqian Liang, Shanshan Zhao, Baosheng Yu, Jing Zhang, and Fazhi He. Meshmae: Masked autoencoders for 3d mesh data analysis. In *European conference on computer vision*, pages 37–54. Springer, 2022. 6
- [51] Yupeng Song, Naifu Liang, Qing Guo, Jicheng Dai, Junwei Bai, and Fazhi He. Meshclip: Efficient cross-modal information processing for 3d mesh data in zero/few-shot learning. *Information Processing & Management*, 60(6):103497, 2023. 6
- [52] Tianchang Shen, Jun Gao, Kangxue Yin, Ming-Yu Liu, and Sanja Fidler. Deep marching tetrahedra: a hybrid representation for high-resolution 3d shape synthesis. *Advances in Neural Information Processing Systems*, 34:6087–6101, 2021. 6
- [53] Ying-Tian Liu, Yuan-Chen Guo, Vikram Voleti, Ruizhi Shao, Chia-Hao Chen, Guan Luo, Zixin Zou, Chen Wang, Christian Laforte, Yan-Pei Cao, et al. threestudio: a modular framework for diffusion-guided 3d generation. *cg. cs. tsinghua. edu. cn*, 2023. 7
- [54] Angel X Chang, Thomas Funkhouser, Leonidas Guibas, Pat Hanrahan, Qixing Huang, Zimo Li, Silvio Savarese, Manolis Savva, Shuran Song, Hao Su, et al. Shapenet: An information-rich 3d model repository. *arXiv preprint arXiv:1512.03012*, 2015. 7
- [55] Jiazheng Xu, Yu Huang, Jiale Cheng, Yuanming Yang, Jiajun Xu, Yuan Wang, Wenbo Duan, Shen Yang, Qunlin Jin, Shurun Li, et al. Visionreward: Fine-grained multi-dimensional human preference learning for image and video generation. *arXiv preprint arXiv:2412.21059*, 2024. 7

A Theoretical Analysis of CS divergence

Theorem 2 (Asymptotic Equivalence). *Suppose Assumption 1 holds. With a constant $C > 0$, the empirical CS divergences $\hat{D}_{\text{CS}}^{\text{paired}}$ and $\hat{D}_{\text{CS}}^{\text{unpaired}}$ computed from paired and unpaired data satisfy:*

$$\left| \hat{D}_{\text{CS}}^{\text{paired}} - \hat{D}_{\text{CS}}^{\text{unpaired}} \right| \leq C \cdot \left(\frac{1}{\sqrt{m}} + \frac{1}{\sqrt{n}} \right) \xrightarrow{p} 0 \quad \text{as } m, n \rightarrow \infty, \quad (10)$$

Here we provide our proof for Theorem 1.

Proof. By Assumption 2(a), we know that the kernel κ is bounded and we have $\sup_{\mathbf{x}} \kappa(\mathbf{x}, \mathbf{x}) \leq K < \infty$, so the canonical feature map φ satisfies $\|\varphi(\mathbf{x})\|_{\mathcal{H}}^2 \leq K$ for all \mathbf{x} .

Next, we define the empirical mean embeddings for the paired and unpaired cases:

$$\boldsymbol{\mu}_x^{\text{paired}} = \frac{1}{m} \sum_{i=1}^m \varphi(r_{\theta_e}(\mathbf{m}_i^+, \mathbf{c}_i)), \quad \boldsymbol{\mu}_y^{\text{paired}} = \frac{1}{m} \sum_{i=1}^m \varphi(r_{\theta_e}(\mathbf{m}_i^-, \mathbf{c}_i)), \quad (11)$$

$$\boldsymbol{\mu}_x^{\text{unpaired}} = \frac{1}{m} \sum_{i=1}^m \varphi(r_{\theta_e}(\mathbf{n}_i^+, \mathbf{c}_i)), \quad \boldsymbol{\mu}_y^{\text{unpaired}} = \frac{1}{n} \sum_{j=1}^n \varphi(r_{\theta_e}(\mathbf{n}_j^-, \mathbf{c}_j)). \quad (12)$$

By the law of large numbers in Hilbert spaces, for i.i.d. samples, we obtain the weak convergence:

$$\frac{1}{m} \sum_{i=1}^m \varphi(r_{\theta_e}(\mathbf{m}_i^+, \mathbf{c}_i)), \frac{1}{m} \sum_{i=1}^m \varphi(r_{\theta_e}(\mathbf{n}_i^+, \mathbf{c}_i)) \xrightarrow{p} \mathbb{E}_{\mathbf{c} \sim p_{\mathbf{C}}, \mathbf{m}^+ \sim p^+(\cdot|\mathbf{c})} [\varphi(r_{\theta_e}(\mathbf{m}^+, \mathbf{c}))], \quad (13)$$

$$\frac{1}{n} \sum_{j=1}^n \varphi(r_{\theta_e}(\mathbf{m}_j^-, \mathbf{c}_j)), \frac{1}{n} \sum_{j=1}^n \varphi(r_{\theta_e}(\mathbf{n}_j^-, \mathbf{c}_j)) \xrightarrow{p} \mathbb{E}_{\mathbf{c} \sim p_{\mathbf{C}}, \mathbf{m}^- \sim p^-(\cdot|\mathbf{c})} [\varphi(r_{\theta_e}(\mathbf{m}^-, \mathbf{c}))]. \quad (14)$$

Thus, we have the convergence of the empirical mean embeddings to their respective population mean embeddings in the RKHS:

$$\boldsymbol{\mu}_x^{\text{paired}}, \boldsymbol{\mu}_x^{\text{unpaired}} \xrightarrow{p} \boldsymbol{\mu}_x^*, \quad \boldsymbol{\mu}_y^{\text{paired}}, \boldsymbol{\mu}_y^{\text{unpaired}} \xrightarrow{p} \boldsymbol{\mu}_y^*, \quad (15)$$

where the population mean embeddings are defined as:

$$\boldsymbol{\mu}_x^* = \mathbb{E}_{\mathbf{c} \sim p_{\mathbf{C}}, \mathbf{m}^+ \sim p^+(\cdot|\mathbf{c})} [\varphi(r_e(\mathbf{m}^+, \mathbf{c}))], \quad \boldsymbol{\mu}_y^* = \mathbb{E}_{\mathbf{c} \sim p_{\mathbf{C}}, \mathbf{m}^- \sim p^-(\cdot|\mathbf{c})} [\varphi(r_e(\mathbf{m}^-, \mathbf{c}))] \quad (16)$$

Applying the triangle inequality for the distance between the paired and unpaired empirical mean embeddings, we obtain:

$$\|\boldsymbol{\mu}_x^{\text{paired}} - \boldsymbol{\mu}_x^{\text{unpaired}}\|_{\mathcal{H}} \leq \|\boldsymbol{\mu}_x^{\text{paired}} - \boldsymbol{\mu}_x^*\|_{\mathcal{H}} + \|\boldsymbol{\mu}_x^{\text{unpaired}} - \boldsymbol{\mu}_x^*\|_{\mathcal{H}} \xrightarrow{p} 0 \quad (17)$$

and similarly for $\boldsymbol{\mu}_y$.

Therefore, the sample means from the paired and unpaired cases converge to the same population mean in RKHS norm. Explicitly, we have:

$$\|\boldsymbol{\mu}_x^{\text{paired}} - \boldsymbol{\mu}_x^{\text{unpaired}}\|_{\mathcal{H}} \xrightarrow{p} 0, \quad \|\boldsymbol{\mu}_y^{\text{paired}} - \boldsymbol{\mu}_y^{\text{unpaired}}\|_{\mathcal{H}} \xrightarrow{p} 0. \quad (18)$$

To quantify the rate of convergence, we apply standard results from the theory of Hilbert space-valued random variables [43]. For all $\varepsilon > 0$:

$$\mathbb{P}(\|\boldsymbol{\mu}_x^{\text{paired}} - \boldsymbol{\mu}_x^*\|_{\mathcal{H}} \geq \varepsilon) \leq 2 \exp\left(-\frac{m\varepsilon^2}{2K}\right), \quad (19)$$

and similarly for $\boldsymbol{\mu}_x^{\text{unpaired}}$.

Therefore, the convergence rate of the difference between the paired and unpaired empirical mean embeddings is given by:

$$\|\boldsymbol{\mu}_x^{\text{paired}} - \boldsymbol{\mu}_x^{\text{unpaired}}\|_{\mathcal{H}} = \mathcal{O}_p\left(\frac{1}{\sqrt{m}}\right). \quad (20)$$

$$\|\boldsymbol{\mu}_y^{\text{paired}} - \boldsymbol{\mu}_y^{\text{unpaired}}\|_{\mathcal{H}} = \mathcal{O}_p\left(\frac{1}{\sqrt{n}}\right). \quad (21)$$

We now consider the empirical CS divergence functional defined as:

$$f(\boldsymbol{\mu}_x, \boldsymbol{\mu}_y) = -2 \log \left(\frac{\langle \boldsymbol{\mu}_x, \boldsymbol{\mu}_y \rangle_{\mathcal{H}}}{\|\boldsymbol{\mu}_x\|_{\mathcal{H}} \|\boldsymbol{\mu}_y\|_{\mathcal{H}}} \right) \quad (22)$$

which is continuous on $\mathcal{H} \setminus \{0\} \times \mathcal{H} \setminus \{0\}$. This condition is satisfied under Assumption 2, which ensures that the population mean embeddings are non-degenerate due to the boundedness and universality of the kernel.

Hence, based on the continuous mapping theorem, we yield:

$$|f(\boldsymbol{\mu}_x^{\text{paired}}, \boldsymbol{\mu}_y^{\text{paired}}) - f(\boldsymbol{\mu}_x^{\text{unpaired}}, \boldsymbol{\mu}_y^{\text{unpaired}})| \xrightarrow{p} 0 \quad (23)$$

That is,

$$\left| \hat{D}_{\text{CS}}^{\text{paired}} - \hat{D}_{\text{CS}}^{\text{unpaired}} \right| \xrightarrow{p} 0 \quad (24)$$

as $m, n \rightarrow \infty$.

Furthermore, under Assumption 2(b), the CS divergence functional $f(\cdot, \cdot)$ is Lipschitz continuous, which allows us to quantify the rate of convergence. Using the previously established rates, we can conclude:

$$|f(\boldsymbol{\mu}_x^{\text{paired}}, \boldsymbol{\mu}_y^{\text{paired}}) - f(\boldsymbol{\mu}_x^{\text{unpaired}}, \boldsymbol{\mu}_y^{\text{unpaired}})| = \mathcal{O}_p\left(\frac{1}{\sqrt{m}} + \frac{1}{\sqrt{n}}\right). \quad (25)$$

Thus, the convergence rate is bounded by:

$$\left| \hat{D}_{\text{CS}}^{\text{paired}} - \hat{D}_{\text{CS}}^{\text{unpaired}} \right| = \mathcal{O}_p\left(\frac{1}{\sqrt{m}} + \frac{1}{\sqrt{n}}\right) \leq C \cdot \left(\frac{1}{\sqrt{m}} + \frac{1}{\sqrt{n}}\right) \quad (26)$$

where C is a constant that depends on the properties of the kernel function and the Lipschitz constant of the empirical CS divergence. \square

B Implementation Details

B.1 Experimental Setup

The conversion of point clouds to meshes was performed using the MeshAnythingV2 framework [32] across 8 L40-S GPUs. For dataset annotation, we employed 4 L40-S GPUs. The training of the reward model, DreamCS, was conducted on 8 x L40-S GPUs using our proposed 3D-MeshPref dataset. The reward model was fine-tuned for 100 epochs using the AdamW optimizer with a learning rate of $1e-3$.

Llama-Mesh Annotation. To annotate the quality of the converted 3D meshes in our dataset, we employ a structured three-criterion annotation rubric. Each criterion is rated on a Likert scale from 0.00 to 5.00, where 5.00 denotes the highest level of performance. The final evaluation score is calculated as the average of the three individual scores:

- **Alignment with the provided description:** Measure the degree to which the 3D mesh accurately reflects the corresponding textual description. Deductions are applied for any semantic misalignment, omission of key elements, or inclusion of irrelevant features.
- **Plausibility and realism of the 3D structure:** Assess the physical plausibility and visual realism of the 3D mesh. Artifacts that violate basic physical principles or render the object visually implausible result in lower scores.
- **Completeness of geometry:** Evaluate the geometric and textural completeness of the 3D mesh. Penalties are applied for missing components, structural incompleteness, or absent/erroneous textures that compromise model integrity.

B.2 Evaluation Pipelines

MiniCPM-o Evaluation. To evaluate the quality of the generated 3D assets across MVDream-based pipelines, we use MiniCPM-o based on a three-part evaluation rubric. Each criterion is rated on a Likert scale from 0.00 to 5.00, where 5.00 denotes the highest performance. The final score is calculated as the average of the three individual scores:

- **Text Prompt and Asset Alignment:** Assess the semantic fidelity between the multi-view renderings and the original textual prompt. The images should depict all referenced entities and contextual elements with accurate visual attributes. Annotators are instructed to first describe the output of each model and then evaluate how comprehensively and accurately the visual content reflects the prompt.
- **3D Plausibility:** Evaluate the inferred 3D structure by examining the set of RGB and normal images. Reviewers consider the overall realism, solidity, and structural coherence implied by the views. Deductions are made for implausible geometry, unnatural proportions, duplicated or floating parts, and any visual artifacts that suggest physical inconsistency. High-quality outputs should convey convincing, well-formed 3D shapes from all angles.
- **Geometry-Texture Alignment:** Measure the local consistency between geometry and texture across views. Specific attention is paid to whether visual features, such as edges, patterns, or object parts, are coherently represented in both RGB and normal maps. Discrepancies between texture and underlying geometry reduce the score.

User Study. To assess the perceptual quality of the generated 3D meshes, we conduct a user study with 30 participants on 30 prompts based on three core criteria across MVDream-based pipelines, as shown in Figures 8 and 9. To avoid bias, models were anonymized, and the response order was randomized. Participants are asked to inspect the 3D meshes from multiple viewpoints and assign a score on a Likert scale from 0.00 to 5.00 for each criterion, where 5.00 denotes the highest performance. The final score is computed as the average of the three individual ratings:

- **Text-Asset Alignment:** Measure how accurately the 3D mesh represents the content described in the original text prompt. Participants assess whether all described objects, attributes, and spatial arrangements are present and correctly rendered in the mesh. Partial or incorrect representations lead to a lower score.
- **3D Plausibility:** Evaluate the realism and structural integrity of the mesh geometry. Participants judge whether the mesh appears physically plausible and free of distortions, unrealistic proportions, or non-functional geometry. 3D meshes with topological errors or unnatural forms are penalized.

- **Geometry-Texture Alignment:** Assess the coherence between the mesh geometry and its texture. Annotators examine whether surface textures appropriately follow the underlying shapes and contours of the geometry. Inconsistencies, such as textures that misalign with surface features or obscure geometric details, result in a lower score.

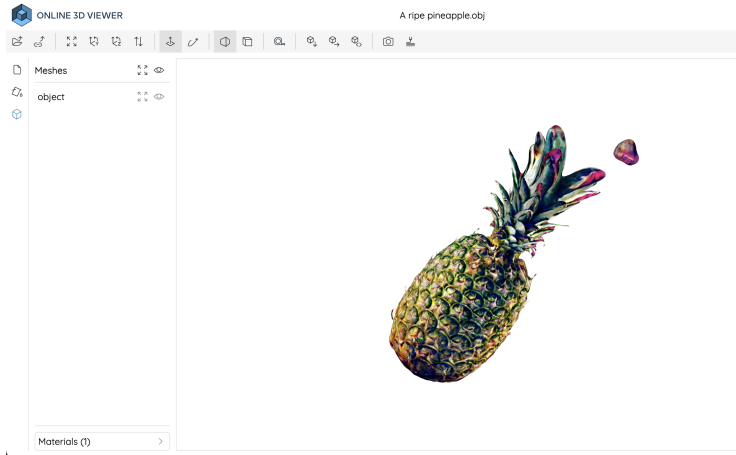


Figure 8: Interface built on Online 3D Viewer used in the user study for evaluating 3D meshes. Participants could interact with the mesh (e.g., rotate, zoom).

User Study

You are presented with a set of 3D meshes generated in response to textual prompts. For each criterion, please assign a score between 0.00-5.00 based on the degree to which the mesh meets the stated objectives.

* Indicates required question

Text-to-Asset Alignment *

Evaluate the fidelity of the 3D mesh to the original text description.

Your answer _____

3D Plausibility *

Assess the physical realism and structural integrity of the mesh.

Your answer _____

Geometry-to-Texture Consistency *

Judge the alignment and coherence between the mesh geometry and its texture.

Your answer _____

Figure 9: User study questionnaire built on Google Form for evaluating 3D mesh quality. Participants can evaluate each mesh based on (1) Text-to-Asset Alignment, (2) 3D Plausibility, and (3) Geometry-to-Texture Consistency.

C More Results

C.1 Qualitative Visualization

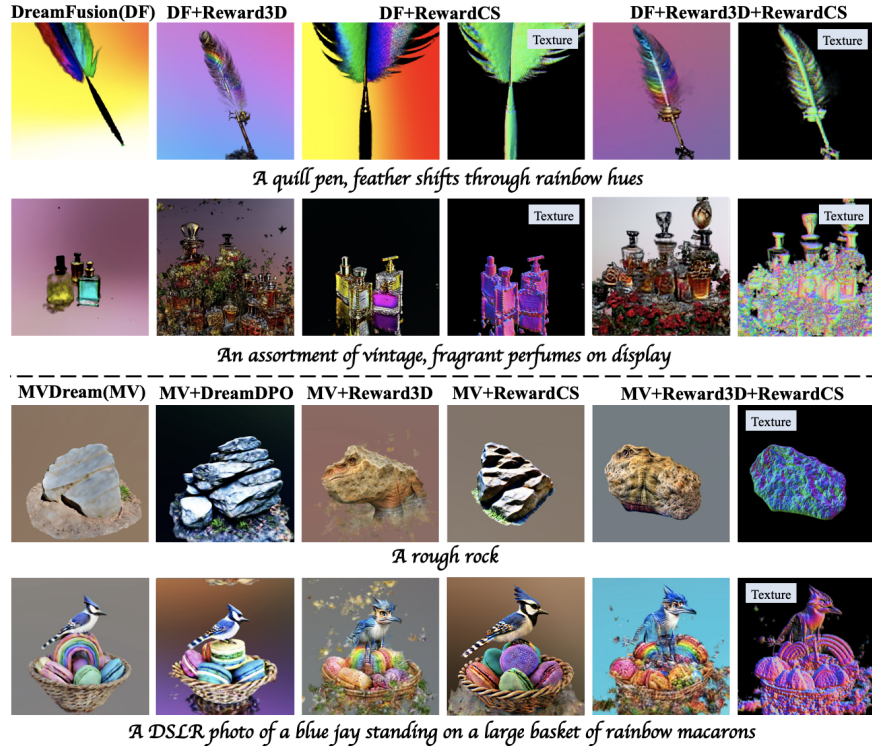


Figure 10: Qualitative comparisons with 1-stage generation pipelines: DreamFusion and MVDream.

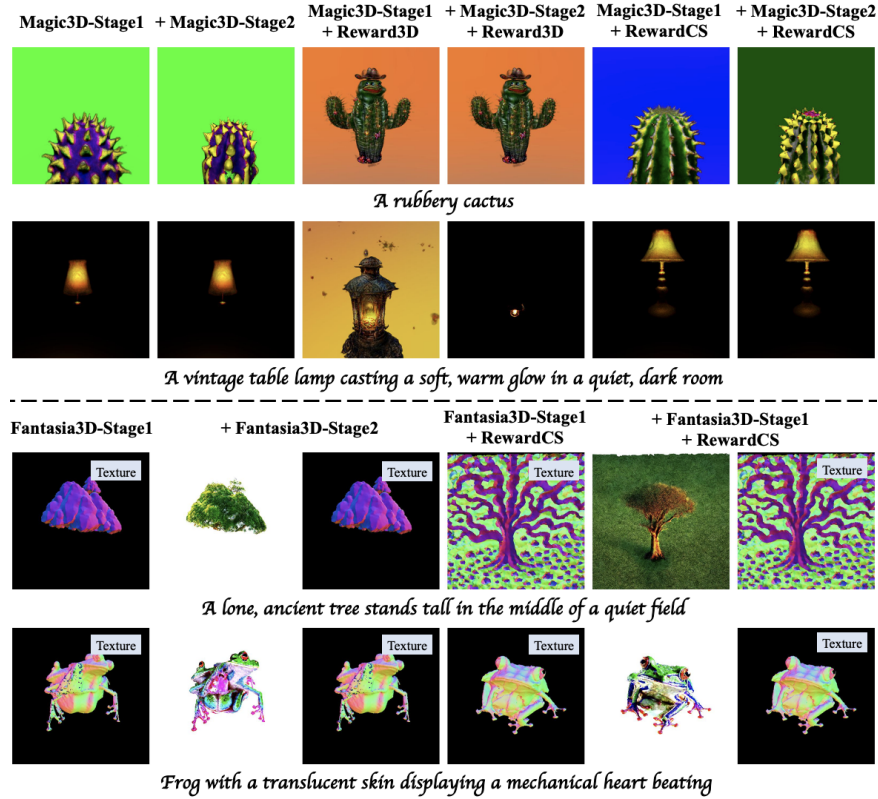


Figure 11: Qualitative comparisons with 2-stage generation pipelines: Magic3D and Fantasia3D.

Figures 10 and 11 demonstrate visualizations of text-to-3D results generated by one-stage and two-stage generation pipelines, respectively. DreamCS outperforms text-to-3D vanilla baselines and variants enhanced with 2D guidance methods, such as DreamReward and DreamDPO, by achieving superior geometric consistency and texture fidelity in 3D generation.

C.2 Quantitative Results

We propose the Geometry-Asset Alignment Reward-XL (GA-XL) metric, derived from RewardCS, which is trained on approximately 10,000 annotated meshes from the Objaverse-XL subset of Cap3D [21]. This metric functions as an independent evaluator for assessing the alignment between 3D mesh geometry and textual descriptions.

Table 4: Comparison of baseline methods using 110 GPTEval3D prompts evaluated with GA-XL under the MVDream backbone.

| Method | GA-XL \uparrow |
|--------------------|------------------|
| MVdream | 2.51 |
| +Reward3D | 2.57 |
| +RewardCS | 2.87 |
| +Reward3D+RewardCS | 2.93 |

As shown in Table 4, RewardCS leads with a GA-XL score of 2.87, surpassing both baseline (2.51) and the variant with 2D guidance (2.57).

D Broader Impact

The text-to-3D base models employed in this research may reflect biases or generate sensitive or potentially offensive 3D content, intended solely for academic and scientific purposes. The opinions expressed within generated outputs do not represent the views of the authors. We remain committed to fostering the development of AI technologies which align with ethical standards and reflect societal values.